SCIENTIFIC REPORTS

OPEN

SUBJECT AREAS:
PAIN
NETWORK MODELS

Received
28 May 2014

Accepted
4 August 2014

Published
2 September 2014

Correspondence and requests for materials should be addressed to A.V.A. (a-apkarian@northwestern.edu)

Resting-sate functional reorganization of the rat limbic system following neuropathic injury

M. N. Baliki, P. C. Chang, A. T. Baria, M. V. Centeno & A. V. Apkarian

Department of Physiology, Northwestern University Feinberg School of Medicine, Chicago, Illinois 60611, USA.

Human brain imaging studies from various clinical cohorts show that chronic pain is associated with large-scale brain functional and morphological reorganization. However, how the rat whole-brain network is topologically reorganized to support persistent pain-like behavior following neuropathic injury remains unknown. Here we compare resting state fMRI functional connectivity-based whole-brain network properties between rats receiving spared nerve injury (SNI) vs. sham injury, at 5 days (n=11 SNI; n=12 sham) and 28 days (n=11 SNI; n=12 sham) post-injury. Similar to the human, the rat brain topological properties exhibited small world features and did not differ between SNI and sham. Local neural networks in SNI animals showed minimal disruption at day 5, and more extensive reorganization at day 28 post-injury. Twenty-eight days after SNI, functional connection changes were localized mainly to within the limbic system, as well as between the limbic and nociceptive systems. No connectivity changes were observed within the nociceptive network. Furthermore, these changes were lateralized and in proportion to the tactile allodynia exhibited by SNI animals. The findings establish that SNI is primarily associated with altered information transfer of limbic regions and provides a novel translational framework for understanding brain functional reorganization in response to a persistent neuropathic injury.

Recent human brain imaging studies show that chronic pain is associated with large-scale brain functional and morphological reorganization[1]. Rodent neuroimaging studies potentially provide a pathway for back-translation of findings from humans to model preparations, wherein more invasive mechanistic experiments can be performed. In rodents, functional magnetic resonance imaging (fMRI) has revealed brain regions related to acute nociceptive processing. The most consistently observed responses are localized to primary and secondary somatosensory cortices, insular cortex, cingulate gyrus, thalamus and periaqueductal gray[2]. However, rodent brain properties that characterize the transition to neuropathic pain remain unknown, and thus it is unclear whether rodent models show appropriate parallels to the human brain reorganization with chronic pain.

Human and rodent brains have complex topological attributes that are thought to provide the physiological basis of information processing[3–5]. Resting-state fMRI (rsfMRI) has been extensively used to map the topological properties of brain networks[6], and importantly it has been determined that these functional properties are susceptible to various pathological disruptions[7]. Unlike conventional evoked-response fMRI, rsfMRI relies on identifying changes in intrinsic fluctuations of the fMRI signal. Given that the brains of chronic pain patients are continuously encoding and processing spontaneous pain, the approach provides a powerful tool with which to detect fundamental aspects of functional brain reorganization associated with chronic pain.

To date, changes in resting-state properties have been observed for multiple chronic pain conditions in humans[8–14]. In contrast, little is known about rsfMRI in animal models of persistent pain. Studies in rodent models of persistent pain show widespread reorganization along the neuraxis[15–17]. Whereas most studies have examined afferent nociceptors and spinal cord pathways, more recent investigations focus on brain circuitry. Various rodent models for persistent pain show morphological, functional, and molecular changes in limbic circuitry, including the hippocampus[18–21], striatum[22–24], frontal cortex[25–27], and amygdala[28]. Based on these results and on recent human imaging data[29,30], we hypothesized that persistent neuropathic pain-like behavior in the rodent is primarily associated with functional reorganization of brain regions within the limbic system, including the hippocampus, amygdala, and striatum. To test this hypothesis, we used rsfMRI to examine the intrinsic reorganization of rat brain functional connectivity following spared nerve injury (SNI). We compared longitudinal changes in topology and functional connectivity of resting-state neural networks between SNI and sham animals following peripheral injury.

Results

SNI animals showed decreased mechanical thresholds at 5 and 28 days post-injury. Consistent with previous observations[31], SNI animals exhibited decreased mechanical thresholds (tactile allodynia) of the injured (left) paw compared to sham at days 5 and 28 post-injury ($F_{1,39} = 85.08$, $p < 0.001$). Additionally, there was no effect of time ($F_{1,39} = 1.09$, $p = 0.30$) nor a group by time interaction ($F_{1,39} = 0.95$, $p = 0.35$). Differences between SNI and sham thresholds at days 5 and 28 post-injury were further assessed using Tukey post-hoc analysis. SNI animals showed significant differences in mechanical threshold of the injured paw at day 5 (mean ± S.D. for SNI = 1.90 ± 0.74; sham = 7.84 ± 0.68; $p < 0.0001$) and at day 28 (SNI = 0.46 ± 0.71; sham = 7.78 ± 0.74; $p < 0.0001$) post-injury. There was no significant within-group difference in mechanical threshold of the injured paw in SNI animals at days 5 and 28 post-injury ($p=0.51$) (Fig. 1a). Finally, SNI animals showed no significant group effect ($F_{1,39} = 1.51$, $p = 0.23$), time effect ($F_{1,39} = 1.17$, $p = 0.29$), nor group by time interaction ($F_{1,39} = 0.78$, $p = 0.38$) in the mechanical thresholds of the uninjured (right) paw.

SNI and sham animals exhibited similar topological properties of brain networks. It remains unknown whether the network organizational principles of the brain are preserved or changed in rodents displaying neuropathic pain-like behavior. Whole-brain resting-state networks were constructed from 96 anatomical ROIs (48 regions in each hemisphere) using a standard rat atlas[32] (Fig. 1b, Table 1), following the methods described in[5] (see methods for details). We compared five global network topological metrics between the SNI and sham animals. These include: 1) clustering, a topological measure of segregated information transfer, 2) global efficiency, a topological measure of integrative information transfer inversely related to characteristic path length, 3) maximum modularity, a global measure of the near-decomposability of the network into a community structure of sparsely interconnected modules, 4) betweenness centrality, which represents the number of shortest paths going through a given node, and 5) small-worldness, based on the tradeoff between clustering and efficiency. Strikingly, all metrics showed no statistically significant differences between the two groups (Fig. 2c–g, Table 2). Finally, the probability distribution of nodal degree (the number of links connecting each node to the network) was best fitted by an exponentially truncated power law. Both the SNI and sham groups exhibited similar degree distributions at day 05 and 28 following neuropathic injury. Thus despite the marked difference in mechanical allodynia between SNI and sham, the brain networks had conserved global properties of small-worldness that were maintained following SNI.

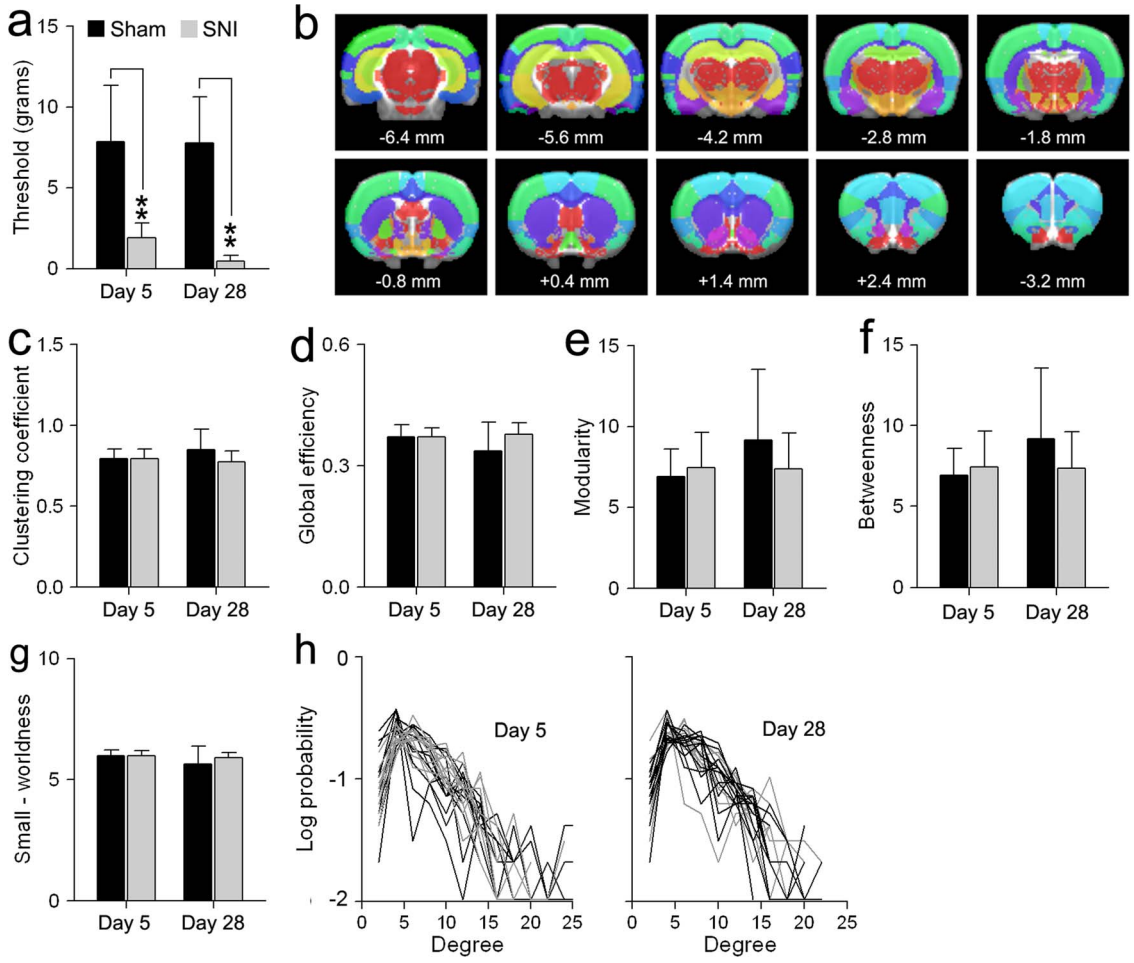

Figure 1 | Global topological features are similar between sham and SNI at 5 and 28 days after injury. (a) Tactile sensitivity threshold of the injured paw in two groups of SNI and sham animals, day 5 (sham: n = 12, SNI: n=11) and day 28 (sham: n = 12, SNI: n= 11) post-injury. Both SNI groups exhibited decreased mechanical threshold compared to sham animals. (b) Colored regions represent anatomically parcellated ROIs (n=96; Table 1). Distance to bregma (in mm) is labeled at the bottom of each slice.(c–g) Topological features including, clustering coefficient, global efficiency, modularity, betweenness centrality, and small-worldness, were similar between SNI and sham animals at both time points post injury. Groups and time differences were evaluated using a two-way ANOVA. (h) Degree distribution, the probability distribution of the degree of a node in the network of sham (black) and SNI (gray) animals 5 and 28 days following injury. Error bars represent S.D. (*p<0.05, ** p<0.01, Tukey post-hoc test).

Table 1 | List of ROIs. All coordinates represents distance from the bregma. X-axis represents the left-right coordinate (right = more positive), y-axis represents the anterior –posterior coordinate (anterior = more positive), z-axis represents the dorsal- ventral coordinates (ventral = more negative). BNST = bed nucleus of the stria terminalis; IPAC = interstitial nucleus of posterior limb of anterior commissure

	ROI number		ROI coordinates (mm)			
ROI name	(left, right)	ROI size (mm^3)	x (left)	x(right)	y	z
Accumbens core	1, 2	3.5	−1.6	1.8	1.4	−6.7
Accumbens shell	3, 4	3.5	−1.4	1.6	1.4	−7.3
Amygdala	5, 6	19.2	−4.1	4.3	−3.5	−8.3
BNST	7, 8	2.2	−1.3	1.5	−0.7	−6.6
Caudate /Putamen	9, 10	40.7	−3.1	3.3	−0.2	−5.2
Corpus collosum	11, 12	28.8	−2.8	2.9	−2.4	−3.3
Auditory cortex	13, 14	12.8	−6.3	6.5	−4.8	−4.3
Cingulate cortex	15, 16	8.3	−0.4	0.6	1.0	−2.3
Entorhinal cortex	17, 18	20.9	−5.4	5.6	−5.0	−7.1
Frontal association cortex	19, 20	4.6	−2.0	2.2	4.8	−2.5
Insular cortex	21, 22	16.1	−5.2	5.4	0.4	−5.8
Medial Prefrontal cortex	23, 24	6.5	−0.5	0.7	2.9	−3.8
Motor cortex	25, 26	40.8	−2.1	2.3	1.6	−1.6
Orbitofrontal cortex	27, 28	11.5	−2.1	2.3	3.8	−4.3
Parietal association cortex	29, 30	5.6	−3.7	3.9	−4.6	−1.5
Piriform cortex	31, 32	21.8	−4.6	4.8	−0.9	−7.8
Retrosplenial cortex	33, 34	14.0	−0.6	0.8	−5.2	−1.6
Somatosensory cortex	35, 36	74.6	−4.4	4.6	−1.1	−2.7
Temporal association cortex	37, 38	5.0	−6.3	6.5	−6.4	−5.0
Visual cortex	39, 40	23.4	−3.8	4.0	−6.4	−1.8
Diagonal band	41, 42	1.8	−0.7	0.9	0.0	−7.8
Globus pallidus	43, 44	3.6	−3.2	3.4	−1.6	−6.3
Hippocampus anterodorsal	45, 46	8.9	−1.5	1.7	−3.2	−3.1
Hippocampus posterior	47, 48	2.0	−3.9	4.1	−6.6	−5.0
Hippocampus posterodorsal	49, 50	16.5	−3.2	3.4	−5.2	−3.6
Hippocampus subiculum	51, 52	10.9	−3.8	4.0	−6.8	−5.1
Hippocampus ventral	53, 54	13.1	−4.5	4.6	−5.3	−6.9
Hypothalamus lateral	55, 55	5.3	−1.5	1.7	−2.7	−8.0
Hypothalamus medial	57, 58	12.1	−0.6	0.8	−3.1	−8.3
Internal capsule	59, 60	7.6	−3.1	3.3	−2.9	−6.1
IPAC	61, 62	1.3	−3.1	3.3	−0.9	−7.4
Medial geniculate	63, 64	1.5	−3.2	3.4	−5.8	−5.5
Mesencephalic region	65, 66	13.6	−1.4	1.6	−6.3	−6.3
Olfactory nuclei	67, 68	5.1	−1.6	1.8	4.3	−5.5
Olfactory tubercle	69, 70	5.7	−1.8	2.0	1.2	−8.3
Periaqueductal grey	71, 72	3.3	−0.4	0.6	−6.7	−5.1
Pons	73, 74	3.6	−0.8	1.0	−7.3	−8.9
Raphe	75, 76	1.0	−0.1	0.3	−6.9	−7.0
Septum	77, 78	6.8	−0.5	0.7	−0.1	−5.2
Substantia innominata	79, 80	2.2	−2.1	2.3	−1.5	−7.7
Substantia nigra	81, 82	3.1	−2.0	2.2	−5.8	−7.2
Superior colliculus	83, 84	9.5	−1.3	1.5	−6.7	−4.0
Thalamus dorsolateral	85,86	20.3	−2.2	2.4	−3.4	−5.2
Thalamus midline dorsal	87, 88	8.0	−0.6	0.8	−3.3	−5.2
Thalamus ventromedial	89, 90	1.7	−0.4	0.6	−2.5	−6.6
Ventral pallidum	91, 92	2.3	−2.1	2.3	−0.1	−7.9
Ventral tegmental area	93,94	1.2	−0.7	0.9	−5.6	−7.7
Zona incerta	95, 96	2.3	−2.1	2.3	−3.9	−6.8

Since different SNI and sham groups were used at days 5 and 28, we assessed the robustness of our results by comparing the Sham groups at days 5 and 28 following injury (unpaired two-tailed t-test). Overall, there were no significant differences between the two sham groups for all topological properties measured including global efficiency (t-value=1.61, p =0.12), clustering coefficient (t-value = −1.40, p =0.14), modularity (t-value = −1.65, p = 0.11), betweenness centrality (t-value = 1.07, p =0.29) and small-worldness (t-value = 1.54, p =0.14).

SNI animals show altered functional connectivity mainly within the limbic system. Specific changes in functional connectivity were revealed by comparing pair-wise ROI connections between the SNI and sham animals ($p < 0.05$, FDR corrected). Five days post-injury, SNI animals exhibited minimal changes in functional connectivity compared to sham (Fig. 2a–b). In contrast, day 28 SNI animals showed a significant number of functional connectivity changes, both increases and decreases (Fig. 2c–d). We investigated these changes within two systems of interest, namely the nociceptive and limbic systems. The nociceptive system encompasses regions shown to be involved in the processing of acute nociceptive information in animals and includes the thalamus, sensorimotor regions (primary motor and sensory cortices), polymodal regions (insula and cingulate), and the periaqueductal gray[2]. The limbic system includes the striatum (accumbens, septum and ventral pallidum), in addition to the amygdala and hippocampus[33]. The regions comprising each system and their corresponding ROIs are listed in Table 3.

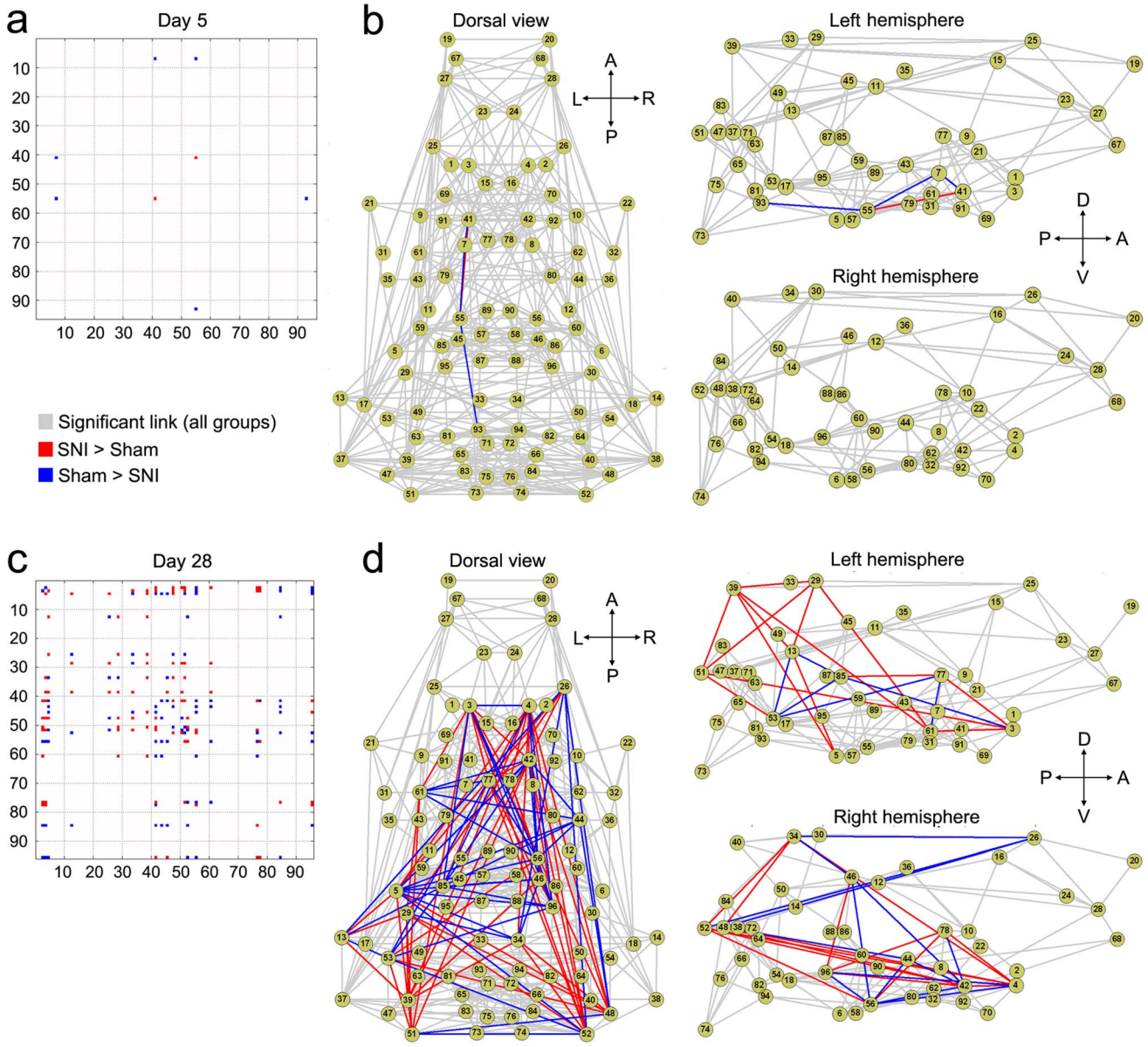

Figure 2 | SNI is associated with late brain functional connectivity reorganization. Matrices show the connections with significantly ($p<0.05$, FDR corrected) stronger (red) and weaker (blue) functional connectivity strength in SNI compared to sham at day 5 (a) and day 28 (c). Connectivity differences between SNI and sham are displayed in the dorsal (top) and lateral views (Left and Right hemispheres separately), at day 5 (b) and day 28 (d). Each node represents the anatomical regions listed in Table 1. Overall, SNI showed robust connectivity changes compared to sham at day 28, but few changes at day 5. (A = anterior; P = posterior; L = left; R = right; V = ventral; D = dorsal).

Table 2 | List of graph metrics. The first column lists the name of the graph metric. Columns two through five list the mean ± S.D. for sham and SNI animals at days 05 and 28. Columns 6–8 list the group, time and group x time effects, respectively. Statistical differences for each graph metric were computed using a two-way ANOVA

	Group (mean ± S.D.)						
Graph metric	Sham (day 5)	SNI (day 5)	Sham (day 28)	SNI (day 28)	Group effect F (p-value)	Time effect F (p-value)	Group x time interaction F (p-value)
Clustering	0.80 ± 0.02	0.79 ± 0.03	0.85 ± 0.02	0.77 ± 0.03	2.69(0.11)	0.51(0.48)	0.51(0.48)
Global efficiency	0.37 ± 0.01	0.37 ± 0.01	0.34 ± 0.01	0.38 ± 0.01	2.70(0.11)	1.32(0.26)	1.32(0.26)
Modularity	6.92 ± 0.82	7.45 ± 0.86	9.17 ± 0.82	7.36 ± 0.86	0.56(0.46)	1.64(0.21)	1.64(0.21)
Betweenness centrality	199.70 ± 9.94	199.12 ± 10.39	183.57 ± 9.94	193.77 ± 10.39	0.22(0.64)	1.12(0.30)	1.12(0.30)
Small-worldness	6.00 ± 0.12	5.98 ± 0.13	5.65 ± 0.12	5.90 ± 0.13	0.83(0.37)	2.95(0.09)	2.95(0.09)

Compared to nociceptive regions, ROIs (nodes) within the limbic systems exhibited larger numbers of connectivity changes (both positive and negative) in SNI compared to sham 28 days following injury (Fig 1a). To better conceptualize the complex pattern of altered functional connectivity, we calculated information flow within and across the seven regions comprising the limbic and nociceptive systems (Table 3). The weight of the edge between two regions was normalized as a percentage of the total number of significantly changed connections between the ROIs (nodes) within two regions ($p < 0.05$ with FDR correction), relative to the total number of all possible connections. Similarly, the node size was normalized relative to the all possible connections within the region (based on the number of possible connection for all ROIs within the region)[5]. The results show that SNI was associated with increased connectivity within the striatum, hippocampus, and amygdala. The striatum showed increased connectivity to thalamus, amygdala, and parts of the hippocampus, as well as to itself. Furthermore, the amygdala showed increased connectivity to sensorimotor areas (Fig 3b). These increases in functional connectivity were coupled with decreases in hippocampal connectivity to thalamic and sensorimotor regions (Fig 3c). Collectively, these results indicate that most functional changes (both increases and decreases) in 28-day SNI animals were either limbic-limbic or limbic-nociceptive in nature (Fig. 3 pie charts). In fact, limbic-limbic connections constituted 72.2% of all significantly increased connections and 39.5% of all decreased functional connections in SNI animals, whereas limbic-nociceptive connections constituted 19.7% and 41.7% of increased and decreased connections, respectively. There were no changes in functional connectivity within the nociceptive system (i.e., nociceptive-nociceptive connections = 0%).

Finally, we investigated differences in pair-wise ROI connections between the sham animals at days 5 and 28 post injury ($p < 0.05$, FDR corrected). The main aims of the analysis were to 1) assess the robustness of our results and 2) identify the changes in brain functional connectivity following acute peripheral injury in the absence of neuropathy. Overall, the two sham groups showed minimal differences in brain functional connectivity. Sham animals at days 5 showed increased connectivity between bilateral amygdala ROIs to the medial and lateral hypothalamus (4 links in total). On the other hand, sham animals at day 28 showed significant increases functional connectivity of right parietal association region to cingulate and right temporal association region (2 links in total).

SNI animals show altered right intra-hemispheric and inter-hemispheric functional connectivity. Global changes in inter- and intra- hemispheric connectivity was examined and compared between SNI and sham animals 28 days following injury. The connectivity strength was computed as the ratio of the total number of significant connections relative to the total number of all possible connections. Significant differences between SNI and sham were assessed using a two-tailed unpaired t-test. SNI showed increased functional connectivity within the right (contralateral to injury) hemisphere (mean ± S.D. for SNI = 0.124 ± 0.008; sham = 0.113 ± 0.012; t-value = 2.31, $p < 0.05$) and decreased inter-hemispheric functional connectivity (SNI = 0.060 ± 0.006; sham = 0.068 ± 0.010; t-value = 2.09, $p < 0.05$). There were no differences in the left intra-hemispheric connectivity between SNI and sham at day 28 (SNI = 0.116 ± 0.009; sham = 0.112 ± 0.013; t-value = 0.964, p = 0.35) (Fig. 4).

In addition, SNI animals showed no significant change in right intra-hemispheric (SNI = 0.119 ± 0.006; sham = 0.119 ± 0.010; t-value = 0.122, p = 0.90), left intra-hemispheric (SNI = 0.118 ± 0.009; sham = 0.117 ± 0.011; t-value = 0.021, p = 0.98), or inter-hemispheric connections (SNI = 0.062 ± 0.008; sham = 0.007 ± 0.011; t-value = 0.062, p = 0.98) at 5 days following injury.

Changes in hippocampus connectivity to sensorimotor and striatal regions reflect pain behavior in SNI. The hippocampus exhibited the strongest changes in functional connectivity between SNI and sham groups at day 28. Here we examined whether these connectivity changes are related to the increased mechanical sensitivity in the SNI group. The connectivity strength of the hippocampus to sensorimotor regions and the striatum was computed as the ratio of the total number of significant connections relative to the total number of all possible connections. In agreement with our initial observations (see Fig. 3), the hippocampus in SNI animals showed significantly increased connectivity to the striatum (mean ± S.D. for SNI = 0.13 ± 0.07; sham = 0.07 ± 0.04; t-value = 2.34, $p < 0.05$), and decreased connectivity to sensorimotor cortex (SNI = 0.04 ± 0.01; sham = 0.09 ± 0.05; t-value = 2.98, $p < 0.01$) at day 28 (Fig. 5). More importantly, these changes in functional connectivity correlated with the decreased mechanical thresholds in the SNI, but not the sham group. The hippocampus connectivity to the striatum showed a strong inverse correlation to paw withdrawal thresholds in the SNI group (r = −0.59, p = 0.05), whereas hippocampal connectivity to sensorimotor regions showed a positive correlation (r = 0.58, p = 0.06). On the other hand, sham animals showed no significant correlation of tactile threshold with hippocampus - striatum connectivity (r = 0.11, p = 0.75), nor with hippocampus-sensorimotor connectivity (r = 0.05, p = 0.89) (Fig 5).

We also investigated differences in hippocampus connectivity strength to the striatum and sensorimotor regions between SNI and sham animals, 5 days post-injury. Surprisingly, the connectivity strength of the hippocampus to the striatum was significantly higher in SNI compared to sham (mean ± S.D. for SNI = 0.09 ± 0.05; sham = 0.05 ± 0.04; t-value = 2.20, $p < 0.05$) and showed an inverse correlation to mechanical thresholds in the SNI group (r = −0.58 p = 0.06). In contrast, the connectivity strength of the hippocampus to sensorimotor cortex did not differ between groups (SNI = 0.11 ±

Table 3 | List of the limbic and nociceptive brain regions. The first column lists the name of the system, the second column lists the major regions within each system and the third column lists the corresponding ROIs. The limbic system included the striatum (accumbens, septum and ventral pallidum), amygdala and hippocampus. The nociceptive system included the thalamus, sensorimotor (primary motor and sensory cortices), polymodal regions (insula and cingulate) and the periaqueductal gray

System	Region	ROIs
Limbic	Striatum	1,2,3,4,77,78,91,92
	Amygdala	5,6
	Hippocampus	45,46,47,48,49,50,51,52,53,54
Nociceptive	Thalamus	85,86,87,88,89,90
	Sensorimotor	25,26,35,36
	Polymodal	15,16,21,22
	Periaqueductal Grey	71,72

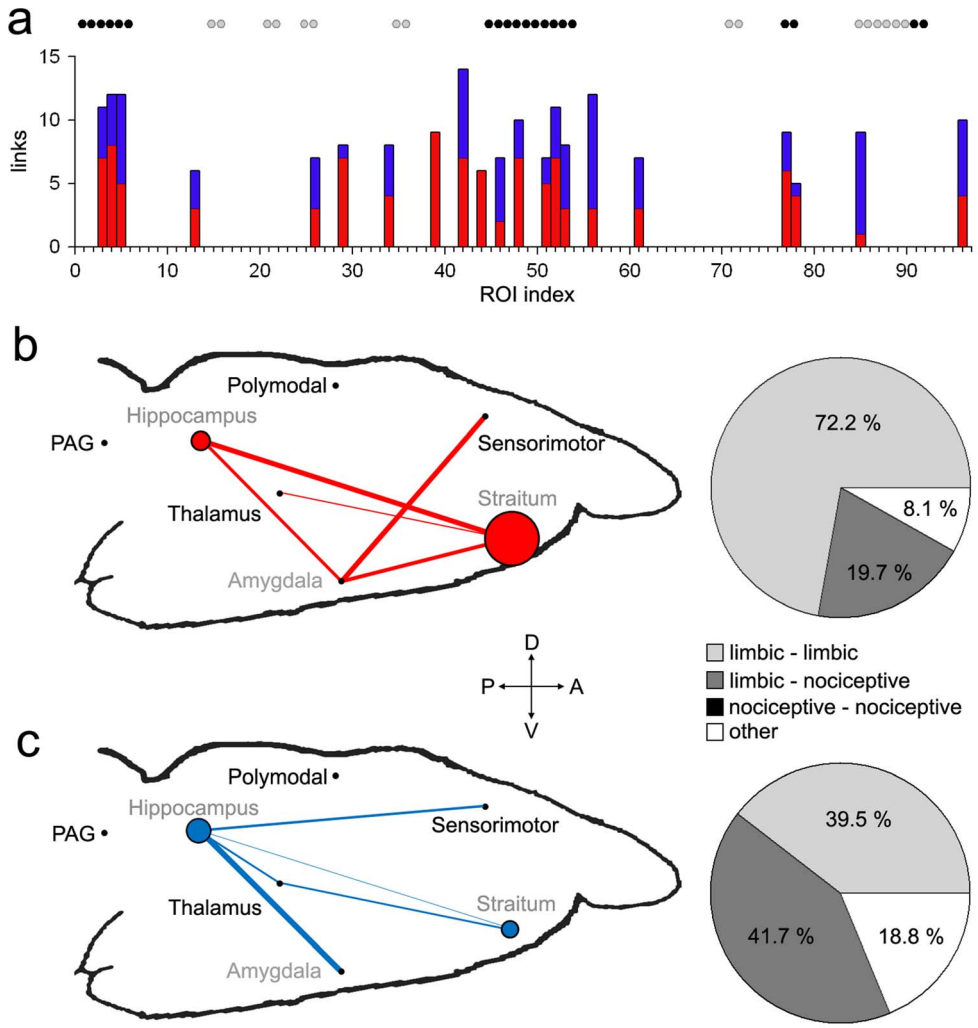

Figure 3 | Functional connectivity changes 28 days after SNI are mainly within limbic, and between limbic and nociceptive regions. (a) Bar graph show the number of significantly decreased (blue) and increased (red) connections for all ROIs in SNI compare to sham 28 days following injury. Black and gray circles denote limbic and nociceptive ROIs respectively. Significantly (b) increased and (c) decreased functional connectivity are shown relative to sham. Limbic (gray labels) and nociceptive (black labels) ROIs were grouped into two separate functional–anatomical modules, labeled at the approximate brain location. Normalized weighted edges and nodes indicate extent of reorganization between and within the seven regions. Pie charts show the percentages of significantly changed limbic and nociceptive connections relative to the total number of changed connections. There were no connectivity differences between nociceptive regions (i.e. nociceptive-nociceptive = 0). See Table 3 for the list of regions and the corresponding ROIs. (A = Anterior; P = posterior; V = ventral; D = dorsal).

0.05; sham = 0.14 ± 0.07; t-value = 1.44, p = 0.16) and was not correlated to mechanical thresholds (r =0.32 p = 0.37).

Discussion

We examined resting state fMRI whole-brain network properties in SNI rats with unilateral partial nerve injuries, at 5 and 28 days after injury, relative to sham operated rats. Our results suggest that functional neural networks are reorganized in SNI animals as a function of time from peripheral injury, and this reorganization is governed by constant topological principles. Although tactile allodynia was robustly present at both 5 and 28 days post-injury, functional connectivity in SNI animals was minimally different from sham at day 5. However, at day 28 SNI animals exhibited both regional increases and decreases in functional connectivity relative to sham. Ninety-seven percent of the observed functional connectivity changes were localized to links within limbic structures, and between limbic and nociceptive structures. Consistent with the anatomy of spino-cephalad projection pathways, we observe increased functional connectivity within the right hemisphere (contralateral to the injury), accompanied by decreased interhemispheric functional connectivity. We also observe increased connectivity between the hippocampus and striatum in SNI animals at both days 5 and 28, and this connectivity reflected the extent of tactile allodynia. On the other hand, connectivity between hippocampus and sensorimotor cortex was absent at day 5 and uncorrelated with tactile allodynia, whereas at day 28, this connection decreased in proportion to tactile allodynia. Thus, we provide the first evidence for time-dependent emergent reorganization of the rodent whole-brain network connectivity with persistence of neuropathic pain, engaging primarily limbic circuitry and limbic-nociceptive interactions, and reflecting the neuropathic pain behavior.

Elsewhere, we have reported on NAc functional connectivity and NAc receptor gene expression in this same cohort of SNI animals[34]. Consistent with the results presented here, minimal NAc connectivity and receptor expression changes were observed at 5 days post-SNI. However, at day 28, connectivity changes in limbic and sensorimotor regions were correlated with dopamine receptor expression, as well as with tactile allodynia. The current results

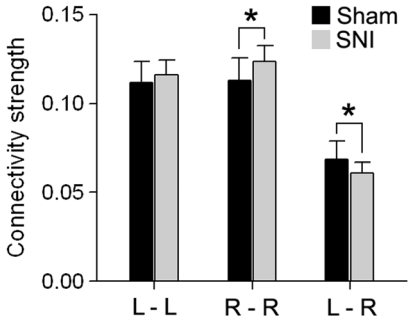

Figure 4 | Functional Connectivity exhibits laterality differences 28 days after SNI. Connectivity strength changes in intra- and inter- hemispheric connectivity in comparison to sham. Connectivity strength was computed as the ratio of the total number of significant connections (at link density = 0.1) relative to the total number of all possible connections. SNI showed increased functional connectivity within the right (contralateral to injury) hemisphere and decreased inter-hemispheric functional connectivity. Error bars represent S.D. (L = left; R = right; *p<0.05, two-sided unpaired t-test).

provide a more global view of the reorganization of this information flow in the brain as neuropathic pain behavior develops.

The most remarkable finding of this study is the specificity of the circuitry that reorganized with persistence of neuropathic pain. Twenty-eight days after SNI, functional connectivity changes were limited to within limbic regions and limbic-nociceptive interactions, with no changes observed within the nociceptive network. The cellular processes driving this reorganization remain to be determined in future electrophysiological studies, yet they highlight the critical role of limbic circuitry in neuropathic pain behavior, and are consistent and complimentary to recent human brain imaging, as well as rodent behavioral and physiological studies. For example, rodents with neuropathic injury exhibit hippocampus-dependent functional impairment[18,21]. In addition, amygdala shows heightened nociceptive information processing, which modulates medial prefrontal (mPFC) excitability, as well as spinal cord excitability[28,35], whereas amygdala lesions inhibit the development of neuropathic pain[36]. Complimentary results have been observed in human studies. For example, the neural substrate underlying pain intensity processing shifts from sensory regions to the amygdala and mPFC as back pain persists to become chronic[37]. Moreover, in humans with chronic pain, NAc phasic activity is abnormal and associated with increased functional connectivity between mPFC and NAc[38], and transition to chronic pain is dependent on information shared between these same regions[29]. Therefore, the four primary nodes of the network that constitutes the mesocorticolimbic circuit, hippocampus, amygdala, striatum, and mPFC, all are implicated in persistent pain.

The current study is the first to comprehensively demonstrate their interactions (except for mPFC), in terms of information shared, in the rodent. The present results are, therefore, entirely consistent with the general theory that we have advanced regarding the critical role of limbic circuitry in persistent pain[39]. This theory posits that the neural circuitry regulating reward and aversion valuation, and appetitive and repulsive motivation, as counterbalanced by emotional decisions resulting in the expression of appropriate behaviors[33], plays a central role in persistent pain. As we observe that hippocampus-striatum connectivity is heightened at day 5, in proportion to tactile allodynia, when the overall brain network shows little reorganization

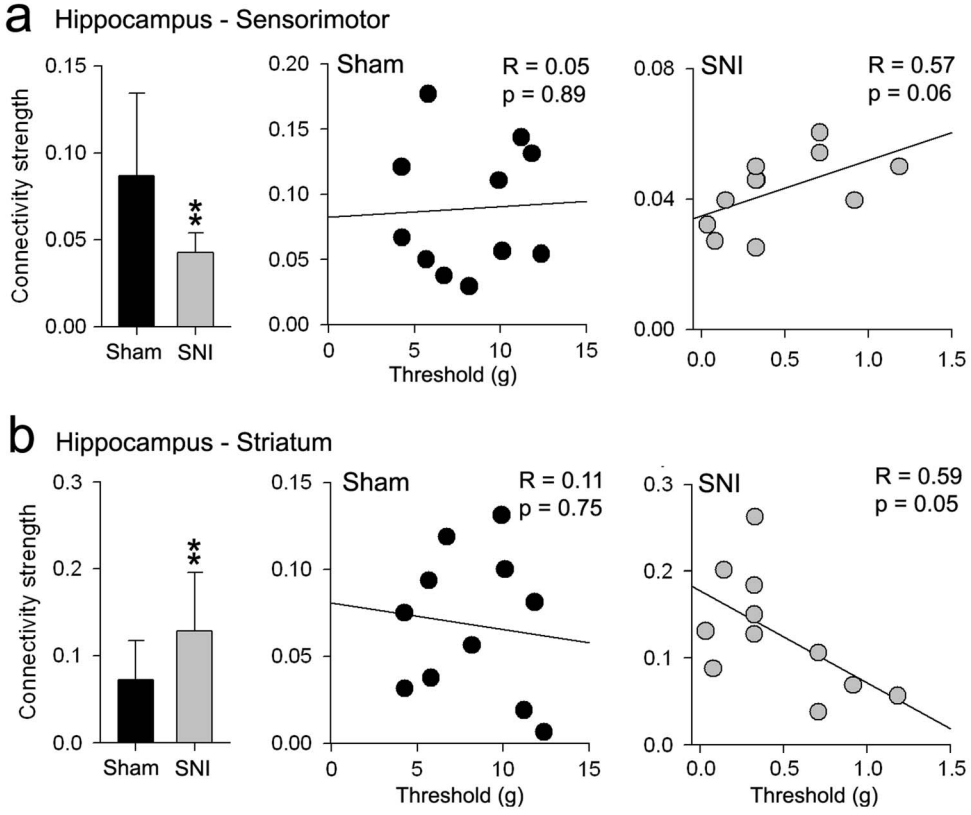

Figure 5 | Changes in hippocampus connectivity to sensorimotor and striatal regions reflect tactile allodynia behavior in SNI. Connectivity strength changes in (a) hippocampus-sensorimotor and (b) hippocampus–striatum connectivity between SNI and sham at day 28. Bar graphs represent the average ratio of the total number of significant connections (at link density = 0.1) relative to the total number of all possible connections between the regions. Scatter plots show the relationship between connectivity strength and tactile sensitivity thresholds of the injured paw in sham (black circles) and SNI (gray circles) animals. Error bars represent S.D. (*p<0.05, **p<0.01, two-sided unpaired t-test).

and this relationship is preserved at 28 days post-peripheral injury, we can conclude that this is an early drive for the later reorganization. Thus, distortions in emotionally-driven limbic circuitry early on after injury, in time, carve the brain to a new state based on associative learning mechanisms[39]. Present results also show that although the limbic connectivity is changing, the nociceptive circuitry remains unperturbed, even though the interaction between the two networks is evident by day 28. Thus, it seems the change in interaction between the two networks is a consequence of the reorganization of the limbic circuit.

Laterality of reorganization of information flow in SNI implies that spino-cephalad pathways are preferentially involved in the reorganization. Spinoparabrachial projections are primarily contralateral in the rat and this pathway provides nociceptive information to the limbic circuitry through monosynaptic projections to the central nucleus of the amygdala[40]. Since we only tested brain network organization for SNI applied to the left paw, we cannot distinguish between hemispheric and afferent laterality. The spinothalamic pathway is the other major spino-cephalad projection with preferential contralateral projections[41,42]. However, the anatomical route for spinothalamic access to limbic circuitry remains unclear. Yet the fact that both sensorimotor and thalamic connectivity to limbic nodes increased in SNI animals implicates the spinothalamic pathway interacting with the limbic network.

The nodes of the nociceptive circuit used in the current study were derived from a review of 31 brain imaging studies in rodents[2], all of which used acute painful stimuli to identify related brain activity. Although the large majority of these studies show activity in somatosensory regions, thalamus, and PAG, many also indicate activity in components of the limbic circuitry studied here, e.g., hippocampus, amygdala, and striatum. Direct comparison of the present results with those in the review is not possible, as the current study examines the brain in the absence of external stimuli. Still, the fact that we observe changes mainly in information flow within limbic and across limbic-nociceptive systems is at odds with the results in the review, given that all of the latter emphasize somatosensory processing of noxious stimuli. The present results are in closer agreement with the human studies wherein brain activity for spontaneous fluctuations of ongoing clinical pain were studied in various chronic pain conditions[1] as well as with resting state studies of chronic pain[8–14].

We should caution, however, that there is no direct information extrapolating the post-injury time window used here and its corresponding timescale in humans as they transition to chronic pain. Still, spinal cord apoptosis is reported to be completed by 3 weeks following neuropathic injury[43], and in a mouse model of pancreatitis, blocking peripheral TRP activity disrupts development of persistent pancreatitis only when administered within 3 weeks from injury, but not at later times[44]. Thus, the brain reorganization we observe 28 days after SNI is at least consistent with the time frame when peripheral interventions lose efficiency and spinal cord reorganization seems stabilized.

The use of anesthesia (isoflurane, a vasodilator) may have dampened mPFC connectivity and reduced our ability to detect expected changes between mPFC and other brain regions in SNI animals. Anesthesia has been reported to alter functional connectivity between brain regions[45,46], including significantly altered thalamocortical connectivity[5], decreased anti-correlated functional connectivity between the infralimbic cortex and amygdala, and an overall decrease in functional connectivity strength[47]. Yet, recent reports show a strong neurovascular coupling in anesthetized rats, indicating that the rsfMRI signal in isoflurane anesthetized rats is mostly of neural origin[48], and that functional connectivity of brain networks maintain topological properties under anesthesia[5].

In conclusion, we observe novel time dependent reorganization of brain information sharing following neuropathic injury. The reorganization mainly impacted the limbic circuitry and this finding has close similarities to recent human brain imaging results for chronic pain and for the transition to chronic pain. Thus, the present results indicate that rodent models show important correspondences to the human pain chronification processes, as such they identify circuit components that may be targeted to modify the transition to chronic pain, and to examine cellular and molecular processes to unravel critical mechanisms that underlie development of chronic pain.

Methods

Animals. A total of 50 adult male Sprague Dawley rats (Harlan, Indianapolis, IN; 200–250 g) were used throughout the experiments. All experiments were approved by and performed in accordance with Northwestern University Institutional Animal Care and Use Committee. Behavioral measures and initial fMRI data analyses were performed in a blinded fashion. Animals were housed on soft bedding in groups of three per cage on a 12-h light/dark cycle in a temperature-controlled environment (21 ± 2°C), with food and water available ad libitum. Handling and testing were performed during the light period. To minimize stress, they were handled regularly before injury and before behavioral testing. Behavioral measures and initial fMRI data analyses were performed in a blinded fashion.

Animals were divided into two groups: one group was tested 5 days after induction of nerve injury (SNI = 12, sham = 12 animals), and a second group was tested 28 days after injury (SNI = 13, sham = 13 animals). Because physiological recording was used for fMRI data pre-processing, rats with incomplete physiological recordings during the scans were excluded from analysis. These include one SNI animal at day 5 and 1 sham animal and 2 SNI animals at day 28. Animals in both groups were sacrificed immediately following behavioral assessment and scanning, and mRNA receptor expression of dopamine 1A, 2, and κ-opioid receptors was quantified in the nucleus accumbens. The mRNA results are reported elsewhere[34].

Spared Nerve Injury (SNI). SNI was used as an animal model of persistent peripheral neuropathic pain. The SNI model has been described previously[31]. Animals were anesthetized with isoflurane (1.5–2%) and a mixture of 30% N_2O and 70% O_2. The sciatic nerve of the left hind leg was exposed at the level of trifurcation into the sural, tibial, and common peroneal nerves. The tibial and common peroneal nerves were tightly ligated and severed, leaving the sural branch intact. Animals in the sham injury group served as the control as their sciatic nerves were exposed, as in the SNI procedure, but they received no further manipulations.

Assessment of mechanical allodynia. Tactile sensitivity of the hind paw was measured using withdrawal responses to a series of von Frey filaments. Animals were placed in a Plexiglass box with a wire grid floor and allowed to habituate to the environment for 10–15 minutes. Filaments of varying forces (Stoelting Co, USA) were applied to the plantar surface of the hind paw. Filaments were applied in either ascending or descending strengths to determine the filament strength closest to the hind paw withdrawal threshold. Each filament was applied for a maximum of 2 seconds at each trial; paw withdrawal during the stimulation was considered a positive response. Given the response pattern and the force of the final filament, 50% response threshold (in grams) was calculated[49]. Paw-withdraw thresholds for 1 SNI animal at day 5 and 2 sham animals at day 28 were not assessed due to technical reasons. Differences in mechanical thresholds of the injured (left) paw between sham and SNI were determined using a two-way ANOVA analysis with group (sham vs. SNI) and time (day 5 vs. day 28) as main effects.

Scanning parameters. All MRI experiments were carried out on a Bruker 7 T/40 cm horizontal magnet (Clinscan, Bruker Biospin, Ettlingen, Germany) with a surface coil. Blood oxygen level-dependent (BOLD) contrast-sensitive T2*-weighted gradient-echo echo-planar images were acquired for resting state fMRI scans. Each scan consisted of 300 volumes of 14 slices acquisition (repetition time (TR) of 1.3 seconds, echo time (TE) of 25 milliseconds, flip angle = 60°, 1.0 mm slice thickness, and 0.5 × 0.5 mm^2 in-plane resolution). A high-resolution T2-weighted RARE anatomical reference was acquired for each animal (1.0 mm slice thickness and 0.273 × 0.273 mm^2 in-plane resolution). An additional T2-weighted RARE anatomical scan with the same geometry as the functional image (1 mm slice thickness and 0.5 × 0.5 mm^2 in-plane resolution) was also acquired and used as a low-resolution anatomical reference.

Anesthesia was induced and maintained during the experiments with isoflurane (1.75–2.5%) mixed with air. Body temperature, respiratory rate, and heart rate were monitored and recorded during scans (Model 1025; SA Instruments, Stony Brook, NY, USA). The monitoring system was operated using a fiber optic temperature probe, respiration pad and fiber optic pulse oxymeter. Respiratory and cardiac waves were recorded during image acquisition with a temporal resolution of 0.001 kHz. To maintain body temperature around 37°C during the imaging session, a feedback-controlled water circulation system (medres, Cologne, Germany) was used to supply the base of the cradle. RsfMRI scans were collected only when physiological parameters remained stable for about 10 minutes.

Data preprocessing. Resting-state fMRI data was preprocessed with AFNI (http://afni.nimh.nih.gov) and FSL 5.1 (FMRIB's Software Library, http://www.fmrib.ox.ac.uk/fsl). The fMRI were first skull stripped and preprocessed using AFNI by applying de-spiking, removal of physiological artifacts from respiration and heartbeat, and

correction for slice timing. The images were then processed using FSL for correction for motion, spatially smoothed with a Gaussian kernel of 0.8 mm FWHM and high pass filtered with a cutoff of 100 seconds. Volumes from functional images were registered to a standard space with a three-step process. Images were first aligned with the individual's low-resolution anatomical image followed by alignment with the individual's high-resolution anatomical image, and then co-registered to a standard space. Average time courses from all of the voxels inside white matter (WM) and cerebrospinal fluid (CSF) were extracted. Confounding regressors that modeled WM and CSF signals and six motion parameters, including translations and rotations, were removed from images through linear regression.

Construction of resting-state functional network. Whole-brain resting-state networks were constructed following the methods described in[5]. Briefly, the rat brain was segmented into 96 anatomical ROIs (48 regions in each hemisphere) using a standard rat atlas[32] (Fig. 1b, Table 1). Averaging the time course of BOLD signal across all voxels within a given ROI generated mean time course for each ROI. Functional correlation was computed using Pearson correlation coefficient between the time courses of each pair of ROIs. Correlation coefficients (i.e., r values) were transformed to z-scores by using Fisher's z transformation, resulting in a 96×96 matrix of normalized correlation coefficients for each subject. Matrices of individual subjects generated in the previous step were subject to density-based thresholding. Network density was defined as the ratio of existing edges to the maximal number of all possible edges in the network that can be estimated as $(N \times (N\text{-}1)/2)$, where N is the number of nodes (ROIs) in the matrix. A link density of 0.1 was used. The network density was selected to 1) ensure that the average degree was not smaller than $2 \times \log(N)$, which guaranteed that the resulting networks were estimable[50], 2) ensure that mean small-worldness (see below for the definition of small-worldness) of the awake brain was not less than 1.5, 3) guarantee that the networks were biologically plausible (in the sense of being small-world networks), and 4) limit the number of spurious edges[5]. Subject specific thresholds were estimated and used to binarize the functional connectivity matrix to zeros (z-scores $<$ threshold $=$ no link) and ones (z-score $>$ threshold $=$ link). This guaranteed that all subject networks contained the same number of links (10% of total possible $=$ 475 links). All subsequent analyses (including graph metrics and connectivity comparisons) were performed on the binarized matrices.

Calculation of graph metrics. Topological measures including clustering coefficient, efficiency, modularity, and betweenness centrality, were computed using the Brain Connectivity Toolbox (BCT, available at https://sites.google.com/a/brain-connectivity-toolbox.net/bct/) in Matla[5]b. Each of these measures, except modularity, is defined at the nodal level; one value is estimated for each node of the graph. Statistical comparisons between groups were made at the global level (i.e., mean of all ROIs). Thus for each animal, one value per measurement was computed and submitted for statistical analysis[5,6]. Furthermore, we computed the 'small-worldness' for each subject based on the tradeoff between clustering and efficiency[51]. A network G is said to be a small-world if $\text{efficiency}_G \leq \text{efficiency}_{random}$ and $\text{clustering}_G \gg \text{clustering}_{random}$. Thus 'small-worldness' for any given network G was computed as $[(\text{clustering}_G / \text{clustering}_{random}) / (\text{efficiency}_{random} / \text{efficiency}_G)]$, where a network is deemed a 'small-world' if resulting value is > 1.5. Random graphs were defined as graphs with the same nodes and number of links (assigned randomly). Efficiency and clustering of random graphs were assessed by averaging along 50,000 random graph permutations. Differences in graph metrics between sham and SNI were determined using a two-way ANOVA analysis with group (sham vs. SNI) and time (day 5 vs. day 28) as main effects.

Connectivity strength. The connectivity strength was compared between the corresponding connections of the SNI and sham conditions using a permutation test[5]. First, for each pair-wise connection, the difference between the means of the two conditions was calculated as the actual group difference. Second, the combined pool of the two conditions was resampled into two new groups. The mean of these two resampled groups was then calculated. This process was repeated 50,000 times to generate a null distribution of the difference of the group mean. The p-value of the actual group difference was calculated as the percentile in the null distribution. Finally, false discovery rate (FDR) correction was performed to correct for multiple comparisons; p-values <0.05 after FDR correction was considered statistically significant.

1. Apkarian, A. V., Baliki, M. N. & Geha, P. Y. Towards a theory of chronic pain. *Prog.Neurobiol.* **87**, 81–97 (2009).
2. Thompson, S. J. & Bushnell, M. C. Rodent functional and anatomical imaging of pain. *Neurosci Lett* **520**, 131–139 (2012).
3. Bullmore, E. & Sporns, O. Complex brain networks: graph theoretical analysis of structural and functional systems. *Nature reviews. Neuroscience* **10**, 186–198 (2009).
4. Fornito, A., Zalesky, A. & Bullmore, E. T. Network scaling effects in graph analytic studies of human resting-state FMRI data. *Frontiers in systems neuroscience* **4**, 22 (2010).
5. Liang, Z., King, J. & Zhang, N. Intrinsic organization of the anesthetized brain. *J Neurosci* **32**, 10183–10191 (2012).
6. Rubinov, M. & Sporns, O. Weight-conserving characterization of complex functional brain networks. *Neuroimage* **56**, 2068–2079 (2011).
7. Bassett, D. S. & Bullmore, E. T. Human brain networks in health and disease. *Curr Opin Neurol* **22**, 340–347 (2009).
8. Tagliazucchi, E., Balenzuela, P., Fraiman, D. & Chialvo, D. R. Brain resting state is disrupted in chronic back pain patients. *Neurosci Lett* **485**, 26–31 (2010).
9. Napadow, V. *et al.* Intrinsic brain connectivity in fibromyalgia is associated with chronic pain intensity. *Arthritis Rheum* **62**, 2545–2555 (2010).
10. Farmer, M. A., Baliki, M. N. & Apkarian, A. V. A dynamic network perspective of chronic pain. *Neurosci Lett* **520**, 197–203 (2012).
11. Cauda, F. *et al.* Altered resting state in diabetic neuropathic pain. *PLoS One* **4**, e4542 (2009).
12. Loggia, M. L. *et al.* Default mode network connectivity encodes clinical pain: An arterial spin labeling study. *Pain* **154**, 24–33 (2012).
13. Ichesco, E. *et al.* Altered functional connectivity between the insula and the cingulate cortex in patients with temporomandibular disorder: a pilot study. *Headache* **52**, 441–454 (2012).
14. Baliki, M. N., Baria, A. T. & Apkarian, A. V. The cortical rhythms of chronic back pain. *J Neurosci* **31**, 13981–13990 (2011).
15. Basbaum, A. I., Bautista, D. M., Scherrer, G. & Julius, D. Cellular and molecular mechanisms of pain. *Cell* **139**, 267–284 (2009).
16. Woolf, C. J. & Salter, M. W. Neuronal plasticity: increasing the gain in pain. *Science* **288**, 1765–1769 (2000).
17. Neugebauer, V., Li, W., Bird, G. C. & Han, J. S. The amygdala and persistent pain. *Neuroscientist.* **10**, 221–234 (2004).
18. Ren, W. J. *et al.* Peripheral nerve injury leads to working memory deficits and dysfunction of the hippocampus by upregulation of TNF-alpha in rodents. *Neuropsychopharmacology* **36**, 979–992 (2011).
19. Al-Amin, H., Sarkis, R., Atweh, S., Jabbur, S. & Saade, N. Chronic dizocilpine or apomorphine and development of neuropathy in two animal models II: effects on brain cytokines and neurotrophins. *Exp Neurol* **228**, 30–40 (2011).
20. del Rey, A. *et al.* Chronic neuropathic pain-like behavior correlates with IL-1beta expression and disrupts cytokine interactions in the hippocampus. *Pain* **152**, 2827–2835 (2011).
21. Mutso, A. A. *et al.* Abnormalities in hippocampal functioning with persistent pain. *J Neurosci* **32**, 5747–5756 (2012).
22. Goffer, Y. *et al.* Calcium-permeable AMPA receptors in the nucleus accumbens regulate depression-like behaviors in the chronic neuropathic pain state. *J Neurosci* **33**, 19034–19044 (2013).
23. Austin, P. J., Beyer, K., Bembrick, A. L. & Keay, K. A. Peripheral nerve injury differentially regulates dopaminergic pathways in the nucleus accumbens of rats with either 'pain alone' or 'pain and disability'. *Neuroscience* **171**, 329–343 (2010).
24. Sarkis, R., Saade, N., Atweh, S., Jabbur, S. & Al-Amin, H. Chronic dizocilpine or apomorphine and development of neuropathy in two rat models I: behavioral effects and role of nucleus accumbens. *Exp Neurol* **228**, 19–29 (2011).
25. Metz, A. E., Yau, H. J., Centeno, M. V., Apkarian, A. V. & Martina, M. Morphological and functional reorganization of rat medial prefrontal cortex in neuropathic pain. *Proc Natl Acad Sci U S A* **106**, 2423–2428 (2009).
26. Seminowicz, D. A. *et al.* MRI structural brain changes associated with sensory and emotional function in a rat model of long-term neuropathic pain. *Neuroimage* **47**, 1007–1014 (2009).
27. Pais-Vieira, M., Aguiar, P., Lima, D. & Galhardo, V. Inflammatory pain disrupts the orbitofrontal neuronal activity and risk-assessment performance in a rodent decision-making task. *Pain* **153**, 1625–1635 (2012).
28. Ren, W., Palazzo, E., Maione, S. & Neugebauer, V. Differential effects of mGluR7 and mGluR8 activation on pain-related synaptic activity in the amygdala. *Neuropharmacology* **61**, 1334–1344 (2011).
29. Baliki, M. N. *et al.* Corticostriatal functional connectivity predicts transition to chronic back pain. *Nat Neurosci* **15**, 1117–1119 (2012).
30. Mansour, A. R. *et al.* Brain white matter structural properties predict transition to chronic pain. *Pain* **154**, 2160–2168 (2013).
31. Decosterd, I. & Woolf, C. J. Spared nerve injury: an animal model of persistent peripheral neuropathic pain. *Pain* **87**, 149–158 (2000).
32. Schwarz, A. J. *et al.* A stereotaxic MRI template set for the rat brain with tissue class distribution maps and co-registered anatomical atlas: application to pharmacological MRI. *Neuroimage* **32**, 538–550 (2006).
33. Volman, S. F. *et al.* New insights into the specificity and plasticity of reward and aversion encoding in the mesolimbic system. *J Neurosci* **33**, 17569–17576 (2013).
34. Chang, P. *et al.* Role of nucleus accumbens in the transition to neuropathic pain. *Pain* **In press** (2014).
35. Bird, G. C. *et al.* Protein kinase A-dependent enhanced NMDA receptor function in pain-related synaptic plasticity in rat amygdala neurones. *J Physiol* **564**, 907–921 (2005).
36. Li, Z., Wang, J., Chen, L., Zhang, M. & Wan, Y. Basolateral amygdala lesion inhibits the development of pain chronicity in neuropathic pain rats. *PLoS One* **8**, e70921 (2013).
37. Hashmi, J. A. *et al.* Shape shifting pain: chronification of back pain shifts brain representation from nociceptive to emotional circuits. *Brain* **136**, 2751–2768 (2013).
38. Baliki, M. N., Geha, P. Y., Fields, H. L. & Apkarian, A. V. Predicting value of pain and analgesia: nucleus accumbens response to noxious stimuli changes in the presence of chronic pain. *Neuron* **66**, 149–160 (2010).
39. Mansour, A. R., Farmer, M. A., Baliki, M. N. & Apkarian, A. V. Chronic pain: The role of learning and brain plasticity. *Restor Neurol Neurosci* **32**, 129–139 (2013).

40. Bernard, J. F., Alden, M. & Besson, J. M. The organization of the efferent projections from the pontine parabrachial area to the amygdaloid complex: a Phaseolus vulgaris leucoagglutinin (PHA-L) study in the rat. *J Comp Neurol* **329**, 201–229 (1993).
41. Kobayashi, Y. Distribution and morphology of spinothalamic tract neurons in the rat. *Anat Embryol (Berl)* **197**, 51–67 (1998).
42. Gauriau, C. & Bernard, J. F. A comparative reappraisal of projections from the superficial laminae of the dorsal horn in the rat: the forebrain. *J Comp Neurol* **468**, 24–56 (2004).
43. Scholz, J. *et al.* Blocking caspase activity prevents transsynaptic neuronal apoptosis and the loss of inhibition in lamina II of the dorsal horn after peripheral nerve injury. *J Neurosci* **25**, 7317–7323 (2005).
44. Schwartz, E. S. *et al.* TRPV1 and TRPA1 antagonists prevent the transition of acute to chronic inflammation and pain in chronic pancreatitis. *J Neurosci* **33**, 5603–5611 (2013).
45. Peltier, S. J. *et al.* Functional connectivity changes with concentration of sevoflurane anesthesia. *Neuroreport* **16**, 285–288 (2005).
46. Boveroux, P. *et al.* Breakdown of within- and between-network resting state functional magnetic resonance imaging connectivity during propofol-induced loss of consciousness. *Anesthesiology* **113**, 1038–1053 (2010).
47. Liang, Z., King, J. & Zhang, N. Anticorrelated resting-state functional connectivity in awake rat brain. *Neuroimage* **59**, 1190–1199 (2012).
48. Liu, X., Zhu, X. H., Zhang, Y. & Chen, W. Neural origin of spontaneous hemodynamic fluctuations in rats under burst-suppression anesthesia condition. *Cereb Cortex* **21**, 374–384 (2011).
49. Chaplan, S. R., Bach, F. W., Pogrel, J. W., Chung, J. M. & Yaksh, T. L. Quantitative assessment of tactile allodynia in the rat paw. *J.Neurosci.Methods* **53**, 55–63 (1994).
50. Watts, D. J. & Strogatz, S. H. Collective dynamics of 'small-world' networks. *Nature* **393**, 440–442 (1998).
51. Humphries, M. D. & Gurney, K. Network 'small-world-ness': a quantitative method for determining canonical network equivalence. *PLoS One* **3**, e0002051 (2008).

Author contributions

A.V.A. designed the research. P.C.C. and M.V.C. performed the behavioral and imaging experiments and collected the data. M.N.B. and A.T.B. implemented the network model and Matlab analysis tools. M.N.B. analyzed the data. M.N.B. and A.V.A. wrote the paper.

Additional information

Competing financial interests: The authors declare no competing financial interests.

How to cite this article: Baliki, M.N., Chang, P.C., Baria, A.T., Centeno, M.V. & Apkarian, A.V. Resting-sate functional reorganization of the rat limbic system following neuropathic injury. *Sci. Rep.* **4**, 6186; DOI:10.1038/srep06186 (2014).